Published online 1 March 2016

Nucleic Acids Research, 2016, Vol. 44, No. 6 ***2491–2500***
doi: 10.1093/nar/gkw083

iSpinach: a fluorogenic RNA aptamer optimized for *in vitro* applications

Alexis Autour, Eric Westhof and Michael Ryckelynck*

Architecture et Réactivité de l'ARN, Université de Strasbourg, Institut de biologie moléculaire et cellulaire du CNRS, 15 rue René Descartes, 67084, Strasbourg, France

Received December 08, 2015; Revised January 29, 2016; Accepted February 01, 2016

ABSTRACT

Using random mutagenesis and high throughput screening by microfluidic-assisted *In Vitro* Compartmentalization, we report the isolation of an order of magnitude times brighter mutants of the light-up RNA aptamers Spinach that are far less salt-sensitive and with a much higher thermal stability than the parent molecule. Further engineering gave iSpinach, a molecule with folding and fluorescence properties surpassing those of all currently known aptamer based on the fluorogenic co-factor 3,5-difluoro-4-hydroxybenzylidene imidazolinone (DFHBI). We illustrate the potential of iSpinach in a new sensitive and high throughput-compatible fluorogenic assay that measures co-transcriptionally the catalytic constant (k_{cat}) of a model ribozyme.

INTRODUCTION

The recent development of new fluorogenic dyes and the concomitant isolation of specific RNA aptamers (1–10) offer the possibility to monitor in real-time the synthesis of a specific RNA both *in vitro* and *in vivo* with applications as diverse as live-cell imaging (11–13), biosensing (14,15) or screening (16). Among this new generation of dyes, the 3,5-difluoro-4-hydroxybenzylidene imidazolinone (DFHBI), a commercially available dye mimicking the natural fluorophore of the green fluorescent protein (17), proved to be particularly well suited for live-cell imaging as it is non toxic, cell membrane-permeable, does not interact with cell components and has a low fluorescence in its free state (18). These attractive properties led to the isolation of a first DFHBI-binding aptamer termed Spinach (6). While Spinach was able to enhance DFHBI fluorescence more than ≈2000 times upon binding, it however suffered from several limitations such as a limited folding efficiency and thermal instability. These limitations were partly overcome in a second version of the aptamer (Spinach2) obtained by rational design (19). Structural studies shed light on the recognition mechanism between the dye and both RNA (20,21) by revealing that both aptamers were built around a G-quadruplex structure and that DFHBI was recognized in a pocket encompassing the top G-quartet, a base triple and a unpaired G residue. The stabilization of this structure requires potassium ions, making the fluorescence of the complex sensitive to the nature of the cation present in the reaction mixture (20,21).

Like every artificial RNA aptamer discovered to date, Spinach was initially isolated by SELEX, a powerful approach to identify specific and high affinity RNA ligand starting from large libraries (22–24) but that does not allow to select for fluorescence phenotypes. Consequently, light-up aptamers are usually identified across a second labor-intensive and low throughput post-selection screening step that allows exploring only a limited fraction of the selected variants. Therefore, as confirmed by a recent study (25), Spinach and its derivatives were likely to be sub-optimal fluorogenic aptamers. This was further supported by a recent work in which FACS-based screening of SELEX-enriched libraries led to the isolation of Broccoli, a DFHBI-binding aptamer optimized for *in vivo* applications with superior stability and fluorescence properties (4).

Beside live-cell imaging applications, several new *in vitro* fluorogenic assays were developed using either the full-length (16,26) or a split version of DFHBI-binding RNA aptamers (27) and Spinach was even used as extracellular metabolite fluorogenic sensor (28). However, despite its great potential, little was known about how well Spinach and its derivatives were adapted to *in vitro* conditions.

In the work presented herein, we show that none of the DFHBI-binding aptamers currently known was optimal for *in vitro* applications since the fluorescence of the complex they generate with DFHBI had a limited thermal stability and strongly depended on the nature of the salt present in the reaction mixture. Using the microfluidic-assisted *In Vitro* Compartmentalization (μIVC) procedure we recently introduced (29) allowed us to screen Spinach gene libraries while applying selection pressures favoring the isolation of aptamers able to work at high temperature and in a potassium free environment. Identified beneficial mutations were combined and the molecule further engineered to afford iSpinach, an aptamer with properties surpassing those

*To whom correspondence should be addressed. Tel: +33 3 88 41 70 55; Fax: +33 3 88 60 22 18; Email: m.ryckelynck@ibmc-cnrs.unistra.fr

© The Author(s) 2016. Published by Oxford University Press on behalf of Nucleic Acids Research.
This is an Open Access article distributed under the terms of the Creative Commons Attribution License (http://creativecommons.org/licenses/by-nc/4.0/), which permits non-commercial re-use, distribution, and reproduction in any medium, provided the original work is properly cited. For commercial re-use, please contact journals.permissions@oup.com

of all DFHBI-binding aptamers described so far. Finally, we demonstrate the potent value of this new aptamer by setting-up a sensitive and high throughput-compatible fluorogenic assay able to assess co-transcriptionally the catalytic constant (k_{cat}) of a model ribozyme.

MATERIALS AND METHODS

Gene library generation

The sequence coding for Spinach 1.1 (19) was flanked with constant regions at 5′ (GGAAGACGTAGCAAG) and 3′ ends (CAGAGAGATGACAGAGAACACA) to afford SpiSel. Mutant libraries were generated by error-prone polymerase chain reaction (PCR) by subjecting 0.04 ng of DNA to 4 amplification cycles in the presence of Rev (TGTGTTCTCTGTCATCTCTCTG) and Fwd (GTAAAACGACGGCCAGTGCCAAGCTTGCATGC-TAATACGACTCACTATAGGAAGACGTAGCAAG) primers as well as nucleotide analogues (JBS dNTP-Mutagenesis Kit, Jena Bioscience) as described before (29). 1 ng of PCR products was amplified in a second PCR mixture containing 10 pmol of each primer (Fwd and Rev), 0.2 mM of each dNTPs, 5 U of DreamTaq™ and the corresponding buffer (Fermentas). The mixture was thermocycled starting with an initial step of denaturation of 2 min at 92°C followed by 4 cycles of: 1 min at 92°C, 1 min at 55°C and 5 min at 72°C, and PCR products were purified. The starting library was TA-cloned and the sequence of 26 clones revealed an average mutation rate of 4.23 mutations per variant.

TA-cloning and sequencing

Genes contained in mutant libraries were diluted in a mixture containing 10 pmol of each primer (Fwd and Rev), 0.2 mM of each dNTPs, 5 U of DreamTaq™ and the corresponding buffer (Fermentas). The mixture was then subjected to an initial denaturation step of 3 min at 95°C, followed by 25 cycles of: 30 s at 95°C, 30 s at 60°C and a final extension step of 10 min at 72°C. PCR products were inserted in pTZ57R/T vector following manufacturer's instructions (InsTAclone PCR cloning Kit, Thermo-Scientific). Ligation products were recovered by phenol/chloroform extraction and 100 ng of DNA used to transform Electro-10 blue bacteria (Agilent) placed in 2 mm electroporation (MicroPulser, Bio-Rad). After an hour of recovery at 37°C under agitation, bacteria were plated on Luria broth (LB)-Amplicillin agar plate and incubated overnight at 37°C. The colonies were picked, used to inoculate liquid LB and grown at 37°C until saturation. Plasmids DNA were extracted using 'GenJet Plasmid Miniprep kit' (Thermo-Scientific), and sequences determined by Sanger approach (GATC Biotech).

Microfluidic chip fabrication and manipulation

The description of the microfluidic devices, their fabrication as well as the microfluidic workstation used in this work can be found in (29).

Microfluidic-assisted *In vitro* Compartmentalization screening

i/ Digital droplet PCR. DNA mutant libraries were diluted in 200 μg/ml yeast total RNA solution (Ambion) down to ≈8 template DNA molecules per picoliter. 1 μl of this dilution was then introduced in 100 μl of PCR mixture containing 20 pmol of each primer (Fwd and Rev), 0.2 mM of each dNTPs, 0.67 mg/ml Dextran-Texas Red 70 kDa (Molecular Probes), 0.1% Pluronic F68, 1x EvaGreen (Biotium), 5 U of DreamTaq™ and the corresponding buffer (Fermentas). The mixture was loaded in a length of PTFE tubing and infused into droplet generator microfluidic chip where it was dispersed in 2.5 pl droplets (production rate of ≈12 000 droplets/s) carried by HFE 7500 fluorinated oil (3M) supplemented with 3% of a fluorosurfactant (29). Droplet production frequency was monitored and used to determined droplet volume, and pumps flow rates (MFCS, Fluigent) adjusted to generate 2.5 pl droplets. Emulsions were collected in 0.2 μl tubes as described before (29) and subjected to an initial denaturation step of 1 min at 95°C followed by 30 cycles of: 1 min at 95°C, 1 min at 55°C, 2 min at 72°C. Droplets were then reinjected into a droplet fusion microfluidic device.

ii/ Droplet fusion. PCR droplets were reinjected and spaced into a fusion device at a rate of ≈1500 droplets/s. Measuring the fraction of droplets with an increased EvaGreen fluorescence allowed assessing droplet occupancy. Each PCR droplet was then synchronized with a 16 pl *in vitro* transcription (IVT) droplet containing 2.2 mM of each NTP (Larova), 24 mM $MgCl_2$, 44 mM Tris-HCl pH 8.0, 5 mM DTT, 1 mM Spermidine, 35 μg/ml of Dextran-Texas Red 70 kDa (Molecular Probes), 0.1% Pluronic F68, 20 μg/ml T7 RNA polymerase, 200 μM DFHBI (Lucerna), 1 μg inorganic pyrophosphatase (Roche) and 50 mM NaCl or KCl. IVT mixture was loaded in a length of PTFE tubing kept on ice during all experiment. PCR droplets were spaced and IVT droplets produced using a single stream HFE 7500 fluorinated oil (3M) supplemented with 2% (w/w) of fluorinated. Flow-rates (MFCS, Fluigent) were adjusted to generate 16 pl IVT droplets and maximize synchronization of 1 PCR droplet with 1 IVT droplet. Pairs of droplets were then fused with an AC field (350 V at 30 kHz) and the resulting emulsion collected off-chip and incubated for 2 h at 37°C.

iii/ Droplet analysis and sort. The emulsion was finally reinjected into of analysis and sorting microfluidic device mounted on Thermo plate (Tokai Hit) holding the temperature at 45°C. Prior to starting droplet fluorescence analysis and sort, the temperature of the microfluidic device was allowed to equilibrate at 45°C for 10 min. The proper warming of the chip was controlled with a thermocouple. The micrometric depth of the channels together with the low droplets re-injection flow rate used were expected to allow equilibration of droplets temperature to that of the device prior to analyzing their fluorescence. Droplets were reinjected at a frequency of ≈200 droplets/s and spaced with a stream of surfactant-free HFE 7500 fluorinated oil (3M). The green fluorescence (DFHBI complexed with the aptamer) of each droplet was analyzed and the 1–2% most green fluorescence droplets were sorted. The gated droplets

were deflected into collecting channel by applying a 1 ms AC fields (1200 V 30 kHz) and collected into a 1.5 ml tube. Residual droplets were recovered from the collection tubing by flushing 200 μl of HFE fluorinated oil (3M). 100 μl of 1H, 1H, 2H, 2H-perfluoro-1-octanol (Sigma-Aldrich) and 200 μl of 200 μg/ml yeast total RNA solution (Ambion) were then added and droplets broken by vortexing the mixture. DNA-containing aqueous phase was then recovered.

Enrichment measurement and colony screening

Genes contained in 2 μl of DNA-containing aqueous phase from unsorted or sorted fractions were placed in 100 μl of PCR mixture identical to that used for TA-cloning and thermocycled starting with an initial cycle of 30 s at 95°C, followed by 25 cycles of: 5 s at 95°C and 30 s at 60°C. Then 2.5 μl of this PCR product were incubated with 16 μl of IVT mixture identical to that used for the μIVC screening containing 200 μM DFHBI but deprived of dextran-Texas Red and pluronic. The transcription mixture was then incubated at 37°C in a real-time thermocycler (Mx 3005P, Agilent) and the green fluorescence (ex: 492 nm/em: 516 nm) measured every minute for 2 h.

Enriched libraries from the last round of screening in the presence of sodium or potassium were TA-cloned. 90 clones were randomly picked, genes coding for the DFHBI-binding aptamers were PCR-amplified and *in vitro* transcribed as for enrichment measurement. Following an hour of transcription real-time monitoring at 37°C, the mutants with the highest apparent transcription rate were sequenced.

RNA synthesis and purification

Genes coding for aptamers of interest were PCR amplified with the same procedure used for enrichment measurements. 20 μl of PCR products were then *in vitro* transcribed in 230 μl of mixture containing 2 mM of each NTP, 25 mM $MgCl_2$, 40 mM Tris-HCl pH 8.0, 5 mM DTT, 1 mM Spermidine and 70 μg/ml T7 RNA polymerase. After 4 h of incubation at 37°C, 10 units of Baseline-Zero™ DNase (Epicentre) and the corresponding buffer were added to the mixture and a second incubation of 1 h at 37°C performed. RNAs was recovered by phenol extraction followed by an ethanol precipitation in the presence of 300 mM sodium acetate pH 5.5 (Sigma-Aldrich). After centrifugation and a wash in 70% ethanol, the pellets were dissolved in denaturing buffer (0.05% bromophenol blue, 0.05% xylene cyanol, 20% glycerol, TBE 1x, 8M urea) and the solution loaded on a 12% denaturing 8 M urea acrylamide/bisacrylamide gel. The piece of gel containing RNA was identified by UV shadowing, sliced from the gel and transferred in a dialyze tube (MWCO = 3500, Spectrum Lab) filled with TBE. RNA was electro-eluted by placing the montage in TBE for 1h00 at 100 V. Eluted RNA were filtered in centrifuge tube 0.45 μm (VWR) and ethanol precipitated in the presence of 300 mM sodium acetate pH 5.5. After centrifugation and a wash in 70% ethanol, the pellets were dissolved in DEPC-Treated water and quantified with Nanodrop (Thermo Scientific).

Fluorescence measurement of purified RNA

A 2 μM solution of purified RNA was heated for 2 min at 85°C and cooled at 25°C for 5 min. The solution was next mixed with 1 volume of a mixture containing 80 mM Tris-HCl pH 7.5, 2 mM $MgCl_2$, 20 μM DFHBI, 200 mM of salt (KCl, NaCl, LiCl or CsCl). The mixture was then incubated at 25°C for 15 min prior to fluorescence measurement. Green fluorescence (ex: 492 nm/em: 516 nm) was then monitored for 5 min at 25°C on a real-time thermocycler (Mx 3005P, Agilent). For T_m^{app} measurement, the temperature was gradually increased from 25 to 60°C with a step of 5°C and a 5 min fluorescence monitoring was performed at each temperature.

Folding efficiency

Folding Efficiency was determined using procedure described in (19). The green fluorescence was measured (ex: 492 nm/em: 516 nm) at three temperatures (25°C, 37°C, 45°C) on a real-time thermocycler (Mx 3005P, Agilent).

Affinity measurements

To measure K_d, the concentration of DFHBI was progressively increased from 100 nM to 200 μM with 100 nM of renatured RNA in 40 mM Tris-HCL pH 7.5, 1 mM $MgCl_2$, 100 mM NaCl or KCl and 2.5% DMSO). The fluorescence was measured (ex: 492 nm/em: 516 nm) at three temperatures (25°C, 37°C, 45°C) on a real-time thermocycler (Mx 3005P, Agilent).

Co-transcriptional k_{cat}^{app} measurement

0.6 pmol of DNA bearing T7 promoter were introduced in 60 μl of mixture containing 40 mM Tris-HCl pH 8.0, 22 mM $MgCl_2$, 5 mM DTT, 1 mM Spermidine, 1,6 mM of each NTP and 65 U/μl T7 RNA polymerase (NEB). 200 pmol of DFHBI or 20 pmol of S21-Atto (29) were then added to 20 μl aliquots and the green fluorescence (ex: 492 nm/em: 516 nm) was monitored for 1h00 at 37°C in a real-time thermocycler (Mx 3005P, Agilent). Fluorescence values were converted into pmol of generated product or synthesized RNA using experimentally measured molar fluorescence of S21-Atto and DFHBI, respectively.

Spectral analysis

Absorbance was measured on a UV-Vis spectrophotometer (Agilent Technology) from 350 nm to 500 nm. Emission (from 410 nm to 60 nm) and excitation (from 350 to 490 nm) was recorded by FluoroMax-4 spectrofluorometer (Horiba Scientific). This measurement was realized using an excess of RNA.

RESULTS AND DISCUSSION

Evaluation of DFHBI-binding aptamers performances *in vitro*

We started our study by characterizing the performances of the three DFHBI-binding aptamers described so far:

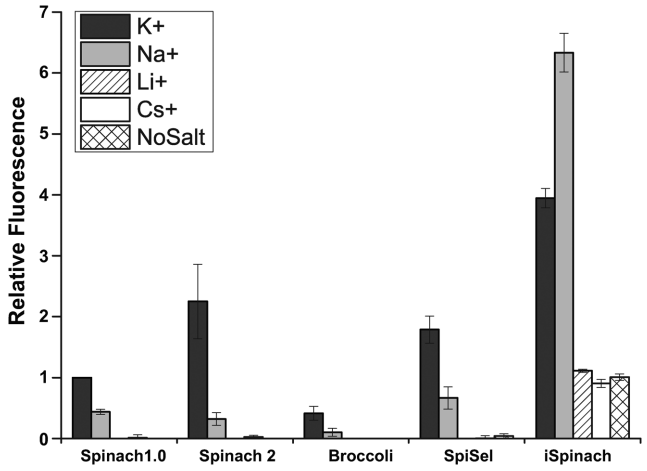

Figure 1. Effect of monovalent cations on the fluorescence of complexes formed between DFHBI and different DFHBI-binding RNA aptamers. 1 μM of RNA was incubated with 10 μM DFHBI in 40 mM Tris-HCl, 1 mM $MgCl_2$ and either 100 mM of salt (K, Na, Li or Cs) or no monovalent cation (no salt). The fluorescence of the complex was measured at 25°C. Values are the mean of three independent experiments and error bars correspond to ± 1 standard error.

Spinach1.0, Spinach2 and Broccoli (4,6,19). To assess unambiguously the intrinsic fluorescence and the folding properties of these molecules, aptamers were used in their minimal version instead of being inserted into a tRNA scaffold (30) as in previously reported (4,19). Coding-genes were *in vitro* transcribed, RNA were gel-purified and renaturated just prior to being used.

First, 10 pmol of aptamer (1 μM) were incubated with 1 nmol of DFHBI in a buffer mimicking *in vivo* conditions (40 mM Tris-HCl pH 7.5, 1 mM MgCl2, 100 mM KCl) and the fluorescence of DFHBI/RNA complexes was measured. As expected from a previous report (19) Spinach2 was twice more fluorescent than Spinach 1.0 in our conditions (Figure 1). Surprisingly, Broccoli, a variant with superior properties *in vivo* (4), generated the dimmest complex with DFHBI *in vitro* (Figure 1). This bad performance was partly explained by a low folding efficiency (F.E. < 18% at 25°C, Supplementary Table S1) of the aptamer in our conditions. A lower F.E. of Broccoli compared to Spinach2 was already suggested in a previous work in which such a strong difference was probably minimized as the aptamer was inserted into a tRNA scaffold that assisted aptamer folding (4). Consequently to this low fluorescence *in vitro*, Broccoli was no longer considered in the rest of the study.

We next investigated the effect of exchanging potassium for another monovalent cation on the fluorescence of DFHBI in complex with Spinach1.0 or 2. Indeed, whereas potassium is the main monovalent cation found *in cellulo* (31), it might not be dominant ion in the extracellular environment and even be absent from *in vitro* reaction mixtures. Using 100 mM NaCl instead of KCl in the reaction mixture led to a significant drop of the fluorescence of both Spinach variants (Figure 1) confirming data previously obtained with Spinach (20). Whereas a residual fluorescence was still observed with sodium, the use of lithium, cesium or the lack of monovalent cation completely abolished the fluorescence of Spinach aptamers (Figure 1). The differential effect of the cations confirmed that proper stabilization of the G-quadruplex motif of the aptamer was necessary for efficient recognition of DFHBI and that the fluorescence of DFHBI/aptamer complex strongly depends on the nature of the monovalent cation present.

Beside the strong dependence of Spinach1.0 and 2 on potassium, both molecules were also reported to have a limited thermal stability as the complexes they generate with DFHBI have melting temperature of ≈34°C and ≈38°C, respectively (19). Accordingly, we found that, in the presence of potassium, the fraction of Spinach2 aptamer properly folded decreased from 61% to 27% at 25°C and 37°C, respectively (Supplementary Table S1).

Overall, these different observations show that none of the DFHBI-binding aptamer described so far was optimized for *in vitro* application (e.g. at 37°C in a reaction mixture not supplemented with potassium). The folding efficiency of the RNA was the main limiting parameter, suggesting that re-evolving the molecule *in vitro* by applying selection pressures favoring the isolation of a thermostable fluorogenic aptamer in a potassium-free environment should lead to the identification of a mutant with properties surpassing those of the rationally designed Spinach2. The use of such conditions that destabilize the molecular folding has already proved to be an efficient strategy as it allowed, for instance, the identification of the Superfolder GFP (32).

Improvement of Spinach properties by *in vitro* evolution

Spinach1.1 was used as starting point of the evolutionary process as its sequence differed from the best variant isolated from SELEX only by a single stabilizing mutation in the basal stem (19). Constant regions were appended at the 5′ of the molecule to ensure a homogeneous transcription initiation and at its 3′ end to enable PCR amplification of the gene. The resulting molecule (SpiSel) was found to have a fluorescence slightly improved (Figure 1). Mutant libraries were then generated by error-prone PCR using a mutation rate of ≈4 mutations per gene and subjected to several rounds of high throughput screening using a procedure of microfluidic-assisted *In Vitro* Compartmentalization (μIVC) we recently developed (29). Even though, this method has a lower throughput than conventional SELEX, it has the great advantage of directly screening libraries for mutants able to generate a fluorescent complex with DFHBI.

Each round of μIVC selection comprised 3 main steps (Figure 2). First, the DNA library was diluted into a PCR mixture down to a concentration of 1 molecule/12.5 pl and the aqueous phase was dispersed into highly monodisperse 2.5 pl droplets carried by a fluorinated oil phase using a first microfluidic device (Figure 2B). The used dilution allowed having, on average, ≈0.2 molecule of DNA per droplet to maximize droplet occupancy (≈18%, Supplementary Table S2) while limiting multiple encapsulation events (<10% of the occupied droplets contained more than 1 gene). Droplets production monitoring was possible by supplementing the PCR mixture with a high concentration of an orange fluorescent dye (670 μg/ml Dextran-Texas

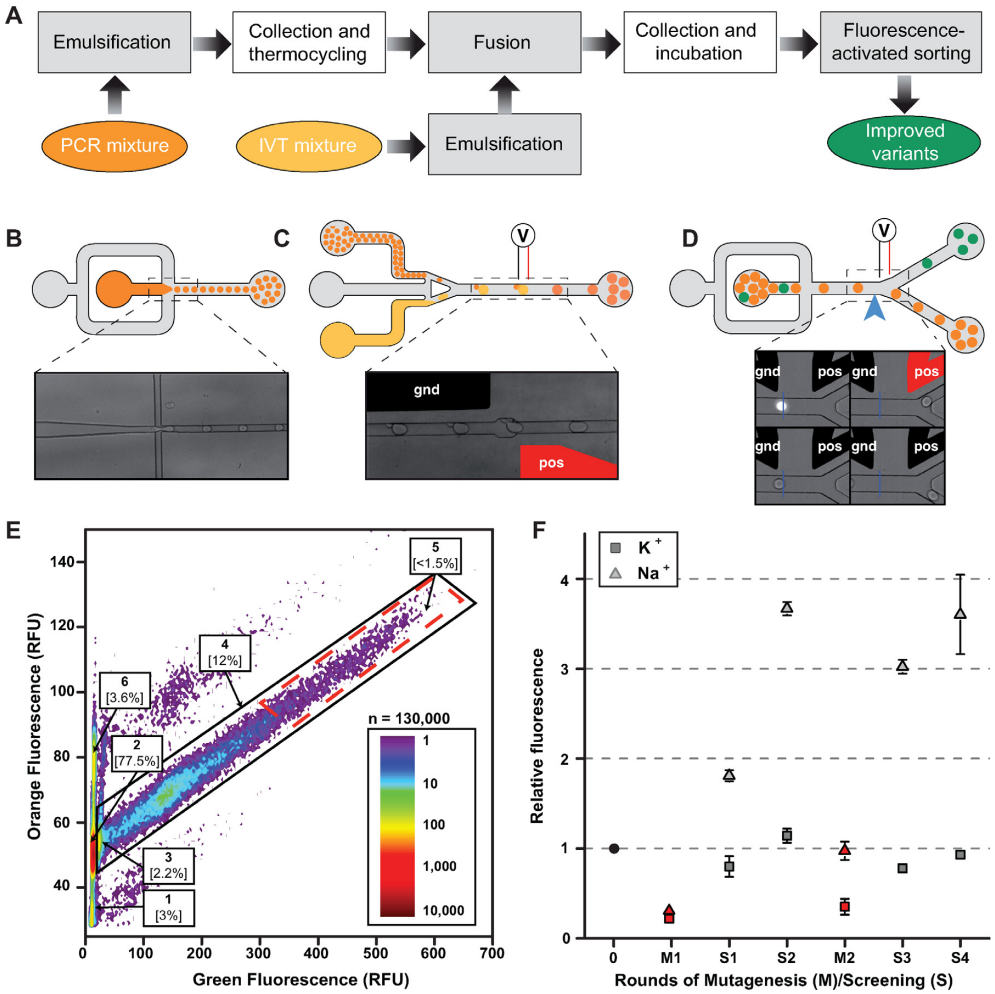

Figure 2. Microfluidic-assisted screening. (**A**) Experimental workflow. Steps performed on-chip (gray boxes) were distinguished from those performed off-chip (white boxes). (**B**) PCR droplets production. Aqueous phase supplemented with a high concentration of a orange fluorescent dye was injected into droplet generator device and 2.5 pl droplets were generated by focusing aqueous (dark orange) and oil (gray) flows. Emulsions were collected and thermocycled. (**C**) Droplets fusion. Small PCR droplets were reinjected into droplet-fusion device and spaced by a stream of oil. 16 pl droplets containing *In Vitro* Transcription (IVT, light orange) mixture supplemented with DFHBI were concomitantly produced and synchronized with PCR droplets. Pairs of droplets were then fused when passing in between a ground-connected electrode (gnd, in black) and an electrode to which tension (pos, in red) was applied. (**D**) Droplets sorting. After incubation, emulsions were reinjected into a Fluorescence Activated Droplet Sorting device and the fluorescence of each droplet read at a detection point (blue arrow and blue line on the micrograph). Based on the fluorescence signal, droplets of interest (green) were deflected into sort channel by applying tension to one of the electrode (pos, in red) whereas non-fluorescent droplets (orange) flowed into the waste channel. (**E**) Typical fluorescence profile of screened emulsion. The analysis of DFHBI green fluorescence and Texas-Red orange fluorescence allowed identifying the different populations composing the emulsion. Indeed, using orange fluorescence signal, IVT droplets fused to single PCR droplets (populations 2–5) were easily discriminated from unfused (population 1) and double fused (population 6) IVT droplets. Green fluorescence resulting from EvaGreen intercalation allowed discriminating droplets containing amplified DNA (population 4) from droplet resulting from fusion with an initially empty PCR droplet (population 2). Finally, the stronger DFHBI green fluorescence allowed discriminating droplets containing non-fluorogenic (population 2) and highly fluorogenic aptamers (population 5, red dashed boxed). Population 5 was gated and corresponding droplets sorted. (**F**) Evolution profiles of SpiSel-derived mutants. Gene libraries obtained after mutagenesis (in red) or screening steps (in gray) were transcribed, the RNAs purified and their fluorogenic properties assayed in the presence of the salt used for the selection. Fluorescence values were normalized to that of SpiSel (black circle) in the same conditions. Screenings performed in potassium (triangles) were distinguished from those performed in sodium (squares). Values are the mean of two independent experiments and error bars correspond to ± 1 standard error.

Red). The emulsion was collected and thermocycled to amplify the DNA prior to reinjecting the droplets into a second microfluidic chip (Figure 2C) where each small droplet was synchronized and fused with an on-chip generated 16 pl droplet containing an *In Vitro* Transcription (IVT) mixture supplemented with 200 μM DFHBI, 50 mM NaCl and a low concentration of the orange fluorescent dye (35 μg/ml Dextran-Texas Red). The new emulsion was collected and incubated. The different concentrations of orange fluorescent dye in PCR and IVT droplets allowed discriminating unfused IVT droplets (low orange fluorescent population 1 on Figure 2E) from IVT droplets fused with 1 (populations 2–5 on Figure 2E) or 2 PCR droplets (population 6 on Figure 2E) and to adjust the flow parameters to maximize the fusion of 1 IVT droplet to 1 PCR droplet (70–92%, Supplementary Table S2). On another hand, the use of sodium was

expected to weaken the G-quadruplex structure while maintaining a residual fluorescence allowing for detecting positive droplets. This was used as a selection pressure favoring the isolation of mutants with improved folding properties. Finally, the emulsion was reinjected into a droplet sorting microfluidic device (Figure 2D) warmed at 45°C, a selection pressure expected to favor the isolation of RNA with improved thermal stability. The orange and green fluorescence of each droplet was measured and the 1% most green fluorescent droplets of the single fused population (population 5 on Figure 2E) were recovered at the end of each round (Supplementary Table S2). To summarize, three selection pressures (use of sodium, sorting device warming and selection of the DFHBI/aptamer complexes based on their brightness) were simultaneously applied to favor the isolation of DFHBI-binding aptamers able to fold efficiently and to form a thermostable fluorescent complex with DFHBI.

A total of two pairs of rounds of selection, interspersed by a round of mutagenesis to maintain genetic diversity, were performed and allowed increasing the average molar fluorescence of the population ≈3.5 times (gray triangles on Figure 2F) with respect to the starting molecule (SpiSel). Interestingly, performing the same *in vitro* evolution experiment using KCl instead of NaCl did not significantly improved the fluorescence of the population after 4 rounds of selection (gray squares on Figure 2F), confirming that sodium was an efficient selection pressure. The enriched library from the fourth round of selection in sodium was then cloned and the fluorescence of 85 individual mutants was analyzed (Supplementary Figure S1). More than 95% of the tested clones were more fluorescent than SpiSel. Whereas the majority of these clones were 2–6 times more fluorescent than SpiSel, the variant 4–68 was surprisingly ≈10 times more fluorescent (Supplementary Figure S1). Sequence analysis (Supplementary Table S3 and Figure S2) revealed that 4–68 differed from SpiSel by 8 mutations (Figure 3A).

Miniaturization and engineering of the improved Spinach

Prior to individually evaluating the contribution of each mutation, we defined the minimal size of 4–68. Indeed, in a previous study Spinach was successfully shortened down to a 51 nucleotides long molecule (BabySpinach) that retained fluorogenic properties (21).

Sequence alignment of the most fluorescent variants revealed that a significant variability (especially deletions) was found in J1/2 (Supplementary Table S3) region indicating a dispensable role of this domain. Accordingly, 4–68-J1/2, a variant deleted of J1/2 (Figure 3B), conserved intact fluorogenic properties (Figure 3E). Conversely, the G-quadruplex domain was strongly conserved and, within the sampled population, only one mutation (A42U) was tolerated (mutant 49 in Supplementary Table S3). Transplanting this mutation into 4–68-J1/2 afforded the variant 4–68/49 (Figure 3C) that conserved identical fluorogenic properties in potassium-containing buffer but had a fluorescence increased ≈3 times in sodium-containing buffer (Figure 3E). This improvement was likely to result from a higher stabilization of the G-quadruplexes in sodium and at 37°C when U was present at this position. Interestingly, a recent thermodynamic-based scanning of Spinach, also identified this mutation as the only one tolerated in this region of the molecule, further supporting our results (25).

The aptamer miniaturization process was pursued by removing 6 base pairs from P3 region to generate a shorter and continuous apical helix (mutant min68). In addition, the first 3 or 6 base pairs of P1 were deleted to generate respectively variants min68/49–3 and min68/49–6 (Figure 3D). While the fluorescence of both constructs remained identical to that of 4–68/49 in the absence of constant regions (Figure 3F), their presence drastically reduced the fluorescence of min68/49–6. Conversely, the fluorescence of the longer variant min68/49–3 was unaffected by the constant regions. Even though more experiments are necessary, it is tempting to propose that the long P1/2 helix of min68/49–3 could act as an insulation module, similar to a three-way junction recently engineered (33), that protects the aptamer from the surrounding sequences.

In addition to A17U (originally A42U), our miniaturized variant (min68/49–3) still contained 6 of the 8 original mutations. U8C and U39C were likely to act by stabilizing RNA structure by converting G.U in stronger G-C base pairs. Mutations A14G and A56G were always found associated together and were the only common feature shared by the two most active mutants (clone 68 and 34 in Supplementary Table S3). To test the contribution of this pair of mutations, we produced a double mutant G14A/G56A and measured its capacity to form a fluorescent complex with DFHBI. Whereas reverting these mutations had only a small effect in the presence of potassium, they drastically reduced the fluorescence in other salts pointing a key role of these mutations in salt resistance of the molecule (Figure 3G). Their location may suggest that these mutations could form a third G-quadruplex with surrounding Gs and, doing so, increase the overall stability of the aptamer. To shed light on the contribution of the two last mutations (C31U and U32C) found in the apical loop of the aptamer, we generated a second double mutant (U31C/C32U) and tested its capacity to form fluorescent complex with DFHBI. Surprisingly, reverting these two positions was found to increase the fluorescence of the complex by ≈25% whereas its salt resistance stayed unchanged (Figure 3G). We considered this double mutant, (U31C/C32U) of min68/49–3, to be the optimal form of the aptamer that could be isolated by our approach and we named it iSpinach.

Performances and applications of iSpinach

We next compared the performances of iSpinach and Spinach2 (Figure 4A). We found that, in addition to being 1.3 times smaller then Spinach2, iSpinach was 1.4 times more fluorescent in potassium (Figure 1). This improvement was likely a combined effect of slightly better folding ability of iSpinach (F.E. ≈70%), a twice-higher affinity for the DFHBI and a slightly increased molar fluorescence of the DFHBI in complex with iSpinach (Figure 4B). We noticed that K_d values obtained with Spinach2 were slightly higher than those from the literature. We attributed this difference to the temperature (25°C) used in our measurements. Indeed, we found that K_d values increased with the temperature (Supplementary Figure S3). However, since

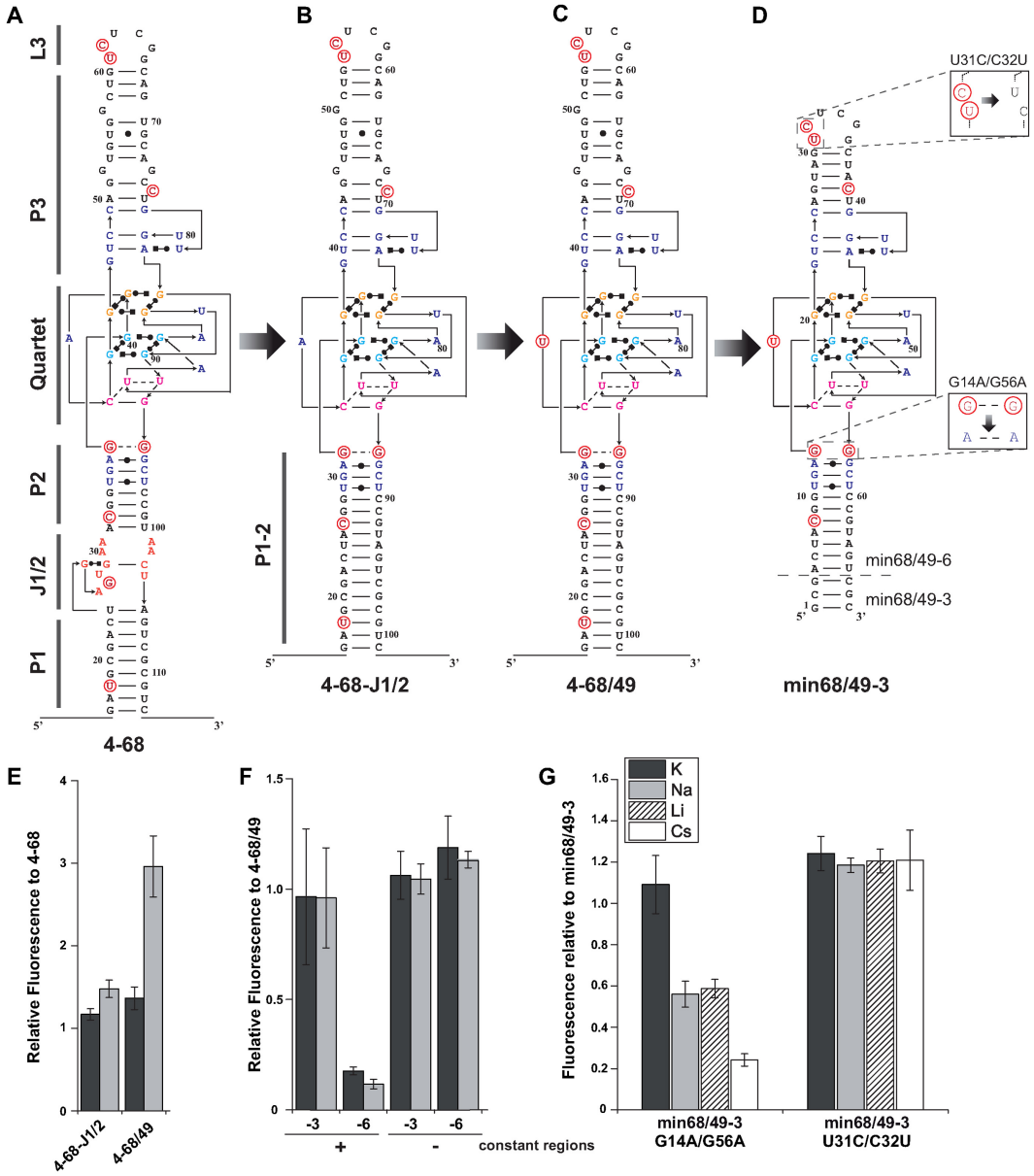

Figure 3. Engineering of improved aptamers. (**A**–**D**) Secondary structure models of aptamers. Molecules are represented according to the model introduced in(21). Mutations are shown in red and numbering adapted to molecule length. (**E**) Effect of J1/2 deletion and A42U mutation on the fluorescence of aptamer 4–68. (**F**) Effect of min68/49 miniaturization on complex fluorescence in the presence or absence of constant regions. Mutant min68/49 was shortened by 3 (−3) or 6 (−6) base pairs. The fluorescence of constructs was tested in the presence and absence of constant regions. (**G**) Effect of double mutations on min68/49–3 fluorescence. The nature of the monovalent cation used is indicated by the color code shown in the inset. Assays were performed with 1 μM RNA and 10 μM DFHBI at 37°C. Values are the mean of three independent experiments and error bars correspond to ± 1 standard error.

none of the previous studies indicated the temperature used to measure this constant, more accurate comparison could not be performed. Finally, iSpinach also formed a more thermostable complex with DFHBI displaying a melting temperature $\left(T_m^{cplx}\right)$ increased by more than 8°C (Figure 4B). iSpinach also outperformed Spinach2 in the presence of lithium and cesium, but we were more surprised to find that the iSpinach/DFHBI complex was not only stable in the presence of sodium but even twice more fluorescent than with potassium (Figure 1). This impressive improvement of the molecule resulted from a better capacity of the aptamer to fold (F.E. ≈ 60%) as compared with Spinach2 leading to an affinity for DFHBI increased by at least an order of magnitude, as well as a doubling of the molar fluorescence of DFHBI (Figure 4B). At this stage, only speculations can be proposed to explain how the nature of the cation affects the brightness of the complex.

The improved folding and fluorescence properties of iSpinach in a wider range of conditions should make it appealing for the design of novel fluorogenic probes as well as of sensitive fluorogenic assays. To demonstrate the advantages that iSpinach may offer, we set-up an *in vitro* experi-

A

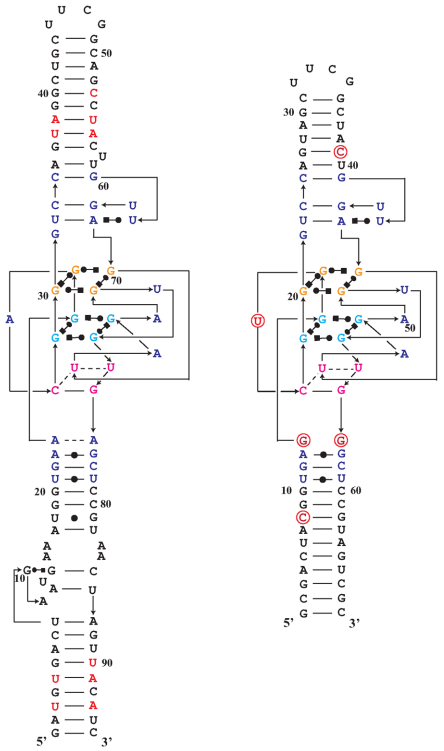

B

	Spinach 2.0		iSpinach	
	K^+	Na^+	K^+	Na^+
F.E. (%)	61.0 ± 12.2	n.d	69.0 ± 4.0	59.6 ± 8.1
T_m^{Cplx} (°C)	36.2 ± 0.2	30.6 ± 0.3	44.6 ± 0.2	36.3 ± 0.10
K_d (μM)	1.45 ± 0.2	>53.4 ± 7	0.92 ± 0.1	4.46 ± 0.2
Max ex. (nm)	445	n.d	442	458
Max em. (nm)	501	n.d	503	507
Rel. Molar Fluo. of DFHBI	1	n.d	1.4 ± 0.1	2.1 ± 0.2

Figure 4. Comparison of Spinach2 and iSpinach. (**A**) Secondary structure models. RNAs were represented according to the model introduced in (21). Mutations are shown in red and numbering adapted to molecule length. (**B**) Aptamers properties. Main parameters including Folding Efficiency (F.E.), melting temperature of the complex $\left(T_m^{cplx}\right)$ and dissociation constant (K_d) of each RNA as well as the Relative Molar Fluorescence of DFHBI were determined at 25°C. Values are the mean of three independent experiments and error bars correspond to ± 1 standard error. Excitation/emission spectra are shown on Supplementary Figure S4.

ment aiming at measuring the apparent catalytic constant $\left(k_{cat}^{app}\right)$ of a ribozyme directly from the *in vitro* transcription mixture. As model ribozyme, we choose iXm1, a variant of X-motif we recently isolated and which transforms its substrate through a simple first order kinetics (29). We fused the DNA coding either for iSpinach, or for Spinach2, to the 3′ end of iXm1 coding region and placed the construct under the control of T7 RNA polymerase promoter sequence (Figure 5A). The resulting gene was then *in vitro* transcribed in a mixture containing a low concentration of T7 RNA polymerase (50 times less than for expression in droplets) to limit the amount of ribozyme generated in the reaction mixture and properly assess k_{cat}^{app} values. In addition, since X-motif was shown not to require monovalent cations (34), the reaction mixture was not supplemented with extra monovalent cations. Upon DNA addition, the reaction mixture was immediately split and mixed with either DFHBI or S21-Atto (a fluorogenic substrate of iXm1(29)) and the fluorescence monitored at 37°C. Ribozyme activity was readily measurable and was not affected by the fusion of the catalyst with fluorogenic aptamers (Figure 5B). Conversely, DFHBI fluorescence was observed only when iSpinach was used alone or fused with iXm1, whereas no fluorescence was observed in the presence of Spinach2 (Figure 5C). The lack of fluorescence of Spinach2-based constructs was attributed to the poor folding performance of the Spinach2 in the experimental conditions used (i.e. potassium-free reaction mixture incubated at 37°C). Spinach2 folding inefficiency could be partly overcome by increasing the potassium concentration up to 100 mM (Figure 1) (20), a concentration of monovalent cations also shown to strongly inhibit T7 RNA polymerase activity (35). Therefore, in addition of being brighter, iSpinach allows to perform experiments in conditions optimal for the activity of the polymerase. The co-transcriptional kinetics of iXm1 activity could be approximated by Equation (1):

$$\frac{dP}{dt} = k_{cat}^{app}\left(\sigma^{rbz} - \delta^{rbz}\right) + k_{uncat} \quad (1)$$

with σ^{rbz} the synthesis rate of the ribozyme, δ^{rbz} its degradation rate and k_{uncat} the substrate auto-hydrolysis rate resulting form T7 RNA polymerase side activity(29). Considering the high efficiency of T7 RNA polymerase, δ^{rbz} was neglected, whereas σ^{rbz} and k_{uncat} were experimentally measured to be 2.1 pmol/min and 0.17 pmol/min respectively and allowed extracting a k_{cat}^{app} value of 0.36 min^{-1}, a value that is close to the 0.48 min^{-1} previously measured with gel-purified RNA (29). This fluorogenic approach can be used to screen ribozyme mutant libraries in high throughput regimes for identifying molecules with high k_{cat}^{app}, but it also demonstrate how the performances of iSpinach is advantageous. In addition, changing the dye labeling the fluorogenic substrate of X-motif for a red emitting one would allow for simultaneously monitoring RNA synthesis (*via* iSpinach fluorescence) and ribozyme activity in a single well.

The present work allowed us to develop iSpinach, a DFHBI-binding aptamer with properties (thermal stability and brightness) surpassing those of Spinach2 and all other DFHBI-binding aptamers in the conditions tested. Isolating this new optimized aptamer was possible by using selection pressures difficult, if not impossible, to apply on living cells (i.e. high temperature, potassium-free environment) but easy to implement *in vitro* using μIVC. In addition, evolving fluorogenic aptamers *in vivo* faces cell-size

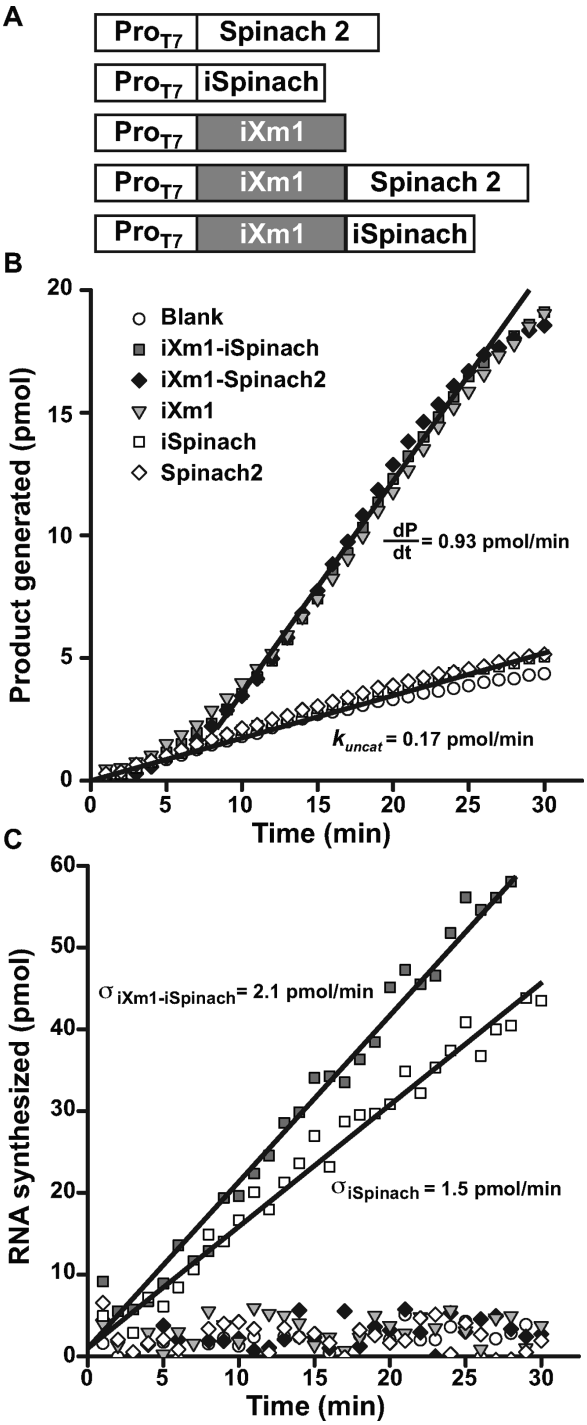

Figure 5. Real-time monitoring of RNA synthesis and ribozyme activity. (**A**) Constructs used. DNA fragments coding for iSpinach, Spinach2 or iXm1 ribozyme were combined in different ways and placed under the control of T7 RNA polymerase promoter sequence (Pro$_{T7}$). (**B**) Real-time ribozyme activity monitoring. The different constructs were *in vitro* transcribed in the presence of ribozyme fluorogenic substrate (S21-Atto) and the fluorescence monitored at 37°C. Product generation rate $\left(\frac{dP}{dt}\right)$ and uncatalyzed reaction rate (k_{uncat}) were determined as the slope of the linear phase of reaction respectively in the presence and absence of ribozyme. (**C**) Real-time transcription monitoring. The *in vitro* transcription mixture used in B. was supplemented with DFHBI (instead of S21-Atto) and the fluorescence monitored at 37°C. The synthesis rate (σ) was determined as the slope of the linear phase.

variations issue making necessary the use of a second fluorescent reporter as internal reference (4), whereas the strong monodispersity (polydispersity < 3% (29)) and homogeneity of the droplets used in μIVC makes this dispensable.

iSpinach acquired several mutations that might have been difficult to predict, especially in the absence of a crystal structure model. Our work shows how powerful *in vitro* evolution may be, provided proper selection pressures and selection format are used. Indeed, whereas Spinach2 was obtained by rational design, the tRNA scaffold-free molecule remained sub-optimal in term of fluorescence and folding stability. In addition, one should also note that none of Spinach2 mutations was found in iSpinach. Recently, an alternative thermodynamic-based approach using large-scale integrated microfluidic chips was introduced to screen libraries of point mutants of Spinach (25). Whereas this technology is extremely powerful at screening small libraries of mutants carrying single mutations, its limited throughput (<1000 mutants per round of screening) makes it less suited at screening more complex libraries (≥2 mutations per molecule). Consequently, even though part of iSpinach mutations were revealed by this methodology, none of them was considered and the improved version of the aptamer was both less thermostable and less fluorescent than iSpinach. The improved properties of iSpinach make it appealing for the development of new *in vitro* applications such as biosensing or high throughput screening. The wider salt-tolerance of iSpinach also makes it a good candidate for the development of new fluorogenic probes working in cellular ionic microenvironments (e.g. endosomes and organelles) to sense their composition (e.g. metabolites, proteins) as this was already described with DNA-based nanodevices (36).

The main limitation of iSpinach and of every other DFHBI-binding aptamers is their low affinity for the DFHBI (K_d > 400 nM) compared to what could be expected. However, Mango RNA was recently isolated and shown to have an affinity 2 order of magnitude higher for its fluorogenic co-factor (K_d ≈3 nM) (10). One can therefore predict that performing SELEX in more stringent selection conditions that favor the isolation of high affinity binders in tandem with μIVC screening should make possible to isolate aptamers able to form bright and high affinity complexes. Finally, Spinach/DFHBI complex was also shown to be prone to light-induced dissociation (37). Since our screening is based on light-induced fluorescence measurement, we anticipate that, in the future, using a stronger light source as well as increasing the illumination time may offer the possibility to isolate new mutants with improved photostability.

SUPPLEMENTARY DATA

Supplementary Data are available at NAR Online.

ACKNOWLEDGEMENTS

We thank Stéphanie Baudrey, Ketty Pernod, Christian Rick and Duygu Yilmaz for technical assistance.

FUNDING

Funding for open access charge: This work has been published under the framework of the LABEX: ANR-10-LABX-0036_NETRNA and benefits from a funding from the state managed by the French National Research Agency as part of the Investments for the future program. It was also supported by the Université de Strasbourg and the Centre National de la Recherche Scientifique.
Conflict of interest statement. None declared.

REFERENCES

1. Arora,A., Sunbul,M. and Jaschke,A. (2015) Dual-colour imaging of RNAs using quencher- and fluorophore-binding aptamers. *Nucleic Acids Res.*, **43**, e144.
2. Babendure,J.R., Adams,S.R. and Tsien,R.Y. (2003) Aptamers switch on fluorescence of triphenylmethane dyes. *J. Am. Chem. Soc.*, **125**, 14716–14717.
3. Constantin,T.P., Silva,G.L., Robertson,K.L., Hamilton,T.P., Fague,K., Waggoner,A.S. and Armitage,B.A. (2008) Synthesis of new fluorogenic cyanine dyes and incorporation into RNA fluoromodules. *Org. Lett.*, **10**, 1561–1564.
4. Filonov,G.S., Moon,J.D., Svensen,N. and Jaffrey,S.R. (2014) Broccoli: rapid selection of an RNA mimic of green fluorescent protein by fluorescence-based selection and directed evolution. *J. Am. Chem. Soc.*, **136**, 16299–16308.
5. Lee,J., Lee,K.H., Jeon,J., Dragulescu-Andrasi,A., Xiao,F. and Rao,J. (2010) Combining SELEX screening and rational design to develop light-up fluorophore-RNA aptamer pairs for RNA tagging. *ACS Chem. Biol.*, **5**, 1065–1074.
6. Paige,J.S., Wu,K.Y. and Jaffrey,S.R. (2011) RNA mimics of green fluorescent protein. *Science*, **333**, 642–646.
7. Pei,R., Rothman,J., Xie,Y. and Stojanovic,M.N. (2009) Light-up properties of complexes between thiazole orange-small molecule conjugates and aptamers. *Nucleic Acids Res.*, **37**, e59.
8. Sando,S., Narita,A., Hayami,M. and Aoyama,Y. (2008) Transcription monitoring using fused RNA with a dye-binding light-up aptamer as a tag: a blue fluorescent RNA. *Chem. Commun.*, **44**, 3858–3860.
9. Sparano,B.A. and Koide,K. (2005) A strategy for the development of small-molecule-based sensors that strongly fluoresce when bound to a specific RNA. *J. Am. Chem. Soc.*, **127**, 14954–14955.
10. Dolgosheina,E.V., Jeng,S.C., Panchapakesan,S.S., Cojocaru,R., Chen,P.S., Wilson,P.D., Hawkins,N., Wiggins,P.A. and Unrau,P.J. (2014) RNA Mango Aptamer-Fluorophore: A Bright, High-Affinity Complex for RNA Labeling and Tracking. *ACS Chem. Biol.*, **9**, 2412–2420.
11. Strack,R.L. and Jaffrey,S.R. (2015) Live-cell imaging of mammalian RNAs with Spinach2. *Methods Enzymol.*, **550**, 129–146.
12. Sunbul,M. and Jaschke,A. (2013) Contact-mediated quenching for RNA imaging in bacteria with a fluorophore-binding aptamer. *Angew. Chem.*, **52**, 13401–13404.
13. Sato,S., Watanabe,M., Katsuda,Y., Murata,A., Wang,D.O. and Uesugi,M. (2015) Live-cell imaging of endogenous mRNAs with a small molecule. *Angew. Chem.*, **54**, 1855–1858.
14. Paige,J.S., Nguyen-Duc,T., Song,W. and Jaffrey,S.R. (2012) Fluorescence imaging of cellular metabolites with RNA. *Science*, **335**, 1194.
15. You,M., Litke,J.L. and Jaffrey,S.R. (2015) Imaging metabolite dynamics in living cells using a Spinach-based riboswitch. *Proc. Natl. Acad. Sci. U.S.A.*, **112**, E2756–E2765.
16. Hofer,K., Langejurgen,L.V. and Jaschke,A. (2013) Universal aptamer-based real-time monitoring of enzymatic RNA synthesis. *J. Am. Chem. Soc.*, **135**, 13692–13694.
17. Chudakov,D.M., Matz,M.V., Lukyanov,S. and Lukyanov,K.A. (2010) Fluorescent proteins and their applications in imaging living cells and tissues. *Physiol. Rev.*, **90**, 1103–1163.
18. You,M. and Jaffrey,S.R. (2015) Structure and Mechanism of RNA Mimics of Green Fluorescent Protein. *Annu. Rev. Biophys.*, **44**, 187–206.
19. Strack,R.L., Disney,M.D. and Jaffrey,S.R. (2013) A superfolding Spinach2 reveals the dynamic nature of trinucleotide repeat-containing RNA. *Nat. Methods*, **10**, 1219–1224.
20. Huang,H., Suslov,N.B., Li,N.S., Shelke,S.A., Evans,M.E., Koldobskaya,Y., Rice,P.A. and Piccirilli,J.A. (2014) A G-quadruplex-containing RNA activates fluorescence in a GFP-like fluorophore. *Nat. Chem. Biol.*, **10**, 686–691.
21. Warner,K.D., Chen,M.C., Song,W., Strack,R.L., Thorn,A., Jaffrey,S.R. and Ferre-D'Amare,A.R. (2014) Structural basis for activity of highly efficient RNA mimics of green fluorescent protein. *Nat. Struct. Mol. Biol.*, **21**, 658–663.
22. Ellington,A.D. and Szostak,J.W. (1990) In vitro selection of RNA molecules that bind specific ligands. *Nature*, **346**, 818–822.
23. Stoltenburg,R., Reinemann,C. and Strehlitz,B. (2007) SELEX–a (r)evolutionary method to generate high-affinity nucleic acid ligands. *Biomol. Eng.*, **24**, 381–403.
24. Tuerk,C. and Gold,L. (1990) Systematic evolution of ligands by exponential enrichment: RNA ligands to bacteriophage T4 DNA polymerase. *Science*, **249**, 505–510.
25. Ketterer,S., Fuchs,D., Weber,W. and Meier,M. (2015) Systematic reconstruction of binding and stability landscapes of the fluorogenic aptamer spinach. *Nucleic Acids Res.*, **43**, 9564–9572.
26. Bhadra,S. and Ellington,A.D. (2014) A Spinach molecular beacon triggered by strand displacement. *RNA*, **20**, 1183–1194.
27. Rogers,T.A., Andrews,G.E., Jaeger,L. and Grabow,W.W. (2015) Fluorescent monitoring of RNA assembly and processing using the split-spinach aptamer. *ACS Synthetic Biol.*, **4**, 162–166.
28. Sharma,S., Zaveri,A., Visweswariah,S.S. and Krishnan,Y. (2014) A fluorescent nucleic acid nanodevice quantitatively images elevated cyclic adenosine monophosphate in membrane-bound compartments. *Small*, **10**, 4276–4280.
29. Ryckelynck,M., Baudrey,S., Rick,C., Marin,A., Coldren,F., Westhof,E. and Griffiths,A.D. (2015) Using droplet-based microfluidics to improve the catalytic properties of RNA under multiple-turnover conditions. *RNA*, **21**, 458–469.
30. Ponchon,L. and Dardel,F. (2007) Recombinant RNA technology: the tRNA scaffold. *Nat. Methods*, **4**, 571–576.
31. Shabala,L., Bowman,J., Brown,J., Ross,T., McMeekin,T. and Shabala,S. (2009) Ion transport and osmotic adjustment in Escherichia coli in response to ionic and non-ionic osmotica. *Environ. Microbiol.*, **11**, 137–148.
32. Pedelacq,J.D., Cabantous,S., Tran,T., Terwilliger,T.C. and Waldo,G.S. (2006) Engineering and characterization of a superfolder green fluorescent protein. *Nat. Biotechnol.*, **24**, 79–88.
33. Filonov,G.S., Kam,C.W., Song,W. and Jaffrey,S.R. (2015) In-gel imaging of RNA processing using broccoli reveals optimal aptamer expression strategies. *Chem. Biol.*, **22**, 649–660.
34. Lazarev,D., Puskarz,I. and Breaker,R.R. (2003) Substrate specificity and reaction kinetics of an X-motif ribozyme. *RNA*, **9**, 688–697.
35. Chamberlin,M. and Ring,J. (1973) Characterization of T7-specific ribonucleic acid polymerase. II. Inhibitors of the enzyme and their application to the study of the enzymatic reaction. *J. Biol. Chem.*, **248**, 2245–2250.
36. Saha,S., Prakash,V., Halder,S., Chakraborty,K. and Krishnan,Y. (2015) A pH-independent DNA nanodevice for quantifying chloride transport in organelles of living cells. *Nat. Nanotechnol.*, **10**, 645–651.
37. Han,K.Y., Leslie,B.J., Fei,J., Zhang,J. and Ha,T. (2013) Understanding the photophysics of the spinach-DFHBI RNA aptamer-fluorogen complex to improve live-cell RNA imaging. *J. Am. Chem. Soc.*, **135**, 19033–19038.